Digital CRISPR Systems for the Next Generation of Nucleic Acid Quantification

Anthony J. Politza[1], Reza Nouri[2], and Weihua Guan[1,2,3*]

[1] Department of Biomedical Engineering, Pennsylvania State University, University Park 16802, USA

[2] Department of Electrical Engineering, Pennsylvania State University, University Park 16802, USA

[3] School of Electrical Engineering and Computer Science, Pennsylvania State University, University Park 16802, USA

* Corresponding Author, Email: wzg111@psu.edu

Abstract

Digital CRISPR (dCRISPR) assays are an emerging platform of molecular diagnostics. Digital platforms introduce absolute quantification and increased sensitivity to bulk CRISPR assays. With ultra-specific targeting, isothermal operation, and rapid detection, dCRISPR systems are well-prepared to lead the field of molecular diagnostics. Here we summarized the common Cas proteins used in CRISPR detection assays. The methods of digital detection and critical performance factors are examined. We formed three strategies to frame the landscape of dCRISPR systems: (1) amplification free, (2) in-partition amplification, and (3) two-stage amplification. We also compared the performance of all systems through the limit of detection (LOD), testing time, and figure of merit (FOM). This work summarizes the details of digital CRISPR platforms to guide future development. We envision that improvements to LOD and dynamic range will position dCRISPR as the leading platform for the next generation of molecular biosensing.

Keywords: Digital CRISPR, CRISPR-Dx, Cas12, Cas13, nucleic acid testing (NAT), DNA Sensing, digital partitioning, absolute quantification

List of Abbreviations:

Cas – CRISPR associated (protein)

CRISPR – Clustered Regularly Interspaced Short Palindromic Repeats

CRISPR-Dx – CRISPR diagnostics

crRNA – CRISPR RNA

dCRISPR – digital CRISPR

dNAAT – digital NAAT

FOM – Figure of merit

gRNA – guide RNA

LAMP – Loop-mediated isothermal amplification

LOD – Limit of detection

NAT – Nucleic acid test

NAAT – Nucleic acid amplification test

PAM – Protospacer adjacent motif

PCR – Polymerase chain reaction

PFS – Protospacer flanking sequence

RPA – Recombinase polymerase amplification

RT-PCR – Reverse transcriptase PCR

RT-LAMP – Reverse transcriptase LAMP

UQL – Upper quantitative limit

1 Introduction

Over the last 40 years, the molecular diagnostic methodology has been dominated by polymerase chain reaction (PCR). The additional developments of heat-stability and reverse transcription via the discovery of *Thermus Aquaticus* and Reverse-Transcriptase, respectively, have securely placed PCR as the gold standard for molecular detection. The benefits of PCR over other platforms include its range of applications, diverse target recognition, assay stability, sensitivity, and specificity [1]. However, PCR is not well suited for rapid testing or in areas of low resources due to the burden of thermal cycling. Therefore, recent assays have attempted to reduce this constraint, thus introducing isothermal amplification methods. These isothermal nucleic acid tests (NATs) have been successful in detecting various nucleic acid targets [2]; however, they lack the specificity and stability of PCR tests [3-5]. Many of these isothermal methods are susceptible to false positives caused by incorrect priming or non-specific fluorescence[5], and therefore, limit the application of these methods for clinical testing. Also, nucleic acid amplification testing still depends on a standard curve for quantification. Therefore, the next generation of molecular diagnostics looks to increase sensitivity and specificity, while maintaining robustness, ease of use, and rapid testing.

Recent developments in the past 10 years have introduced Clustered Regularly Interspaced Short Palindromic Repeats (CRISPR) systems as an ultra-specific and rapid form of molecular diagnostics [6-10]. These systems have shown incredibly high binding specificity and targeted cleavage for DNA and RNA targets in under one hour [11-14]. These CRISPR diagnostics (CRISPR-Dx) systems repurpose the same toolkit that gene editing CRISPR systems use. There is a CRISPR-associated (Cas) protein that enzymatically cuts target nucleic acids at specific sequences. The Cas protein is directed to these sequences when bound to a CRISPR RNA (crRNA) that explicitly complements the nucleic acid sequence of the target. Once the Cas-crRNA complex is bound to the target, the Cas precisely slices the target strand [9, 15]. This CRISPR activity was first discovered in prokaryotes as a simple adaptive immune system against invading virus genomes. As you can infer, this precise slicing appealed greatly to gene editing applications where targeted strand cuts are needed for gene knockouts or replacement [16]. For diagnostics, systems of detection with Cas9 were developed but remained limited due to their complex setups and non-trivial readout methods.

In 2016, the discovery of collateral cleavage from several newer Cas proteins truly expanded

the future of CRISPR-Dx. Newer Cas proteins, such as Cas12, Cas13, and Cas14, are still Class II CRISPR proteins ; however, Cas12 through 14 have demonstrated unbiased cleavage of neighboring nucleic acids, in addition to their specific targets. Therefore, the discovery of collateral cleavage alleviated the complexities seen in Cas9 detection systems. Non-specific cleavage could now be used with fluorescent or lateral-flow reporters. With this knowledge, many systems have been able to detect SARS-Cov-2, DENV, and Zika viruses using FAM-quencher or FAM-biotin arrangements for fluorescent and lateral-flow readouts, respectively [11-14, 17]. These systems provide a benefit over isothermal amplification systems alone as they counter the issue of false positives with target-specific detection. In fact, CRISPR-Dx systems have three distinct binding regions that must be satisfied before the cleavage occurs (crRNA-Cas, crRNA-target, and Cas-target by PAM or PFS). However, they still require as much time as traditional amplification or even more while being more cumbersome to handle and process. Therefore, to compete against PCR, CRISPR needs improvements to decrease the limits of detection and reduce assay time.

The most sensible method of improving CRISPR assays on both issues is to use digitalization [18]. In our previous study, we developed a figure of merit (FOM) for CRISPR sensing [19]. By comparing CRISPR assays with multiple crRNA, sensitive readout systems, digital methods, and amplification, digital assays showed the greatest improvement. The addition of digital partitioning offers two advantages. It inherently boosts the limit of detection (LOD) of the system and therefore eliminates the need for pre-amplification, which drastically reduces the time requirement for testing. Additionally, digital methods provide absolute quantification. Therefore, removing the need for a standard curve. Digital methods also offer the potential for expanded dynamic range through multiplexing and ease of expansion. Last, digitalization presents a method for single molecule characterization and could provide the CRISPR field with an alternative to bulk measurements. So far, studies have successfully consolidated CRISPR into digital systems. However, to compete as the next generation of molecular diagnostics, dCRISPR systems need improvement in robustness, usability, and automation to match the advances that nucleic acid amplification has made over the last two decades. The culmination of these improvements inside a well-engineered system presents digital CRISPR (dCRISPR) as the next generation of molecular diagnostics that are more rapid, sensitive, and specific than current amplification methods.

Here in this work, we review the current landscape of dCRISPR to compare differences

between Cas proteins, their targets, and the methods required to utilize them inside a diagnostic system. First, we summarize the top CRISPR-Dx proteins to condense information for future studies. Next, we review the principles of digitalization and the factors affecting performance. Third, we compare the current digital CRISPR configurations being employed today. Last, we summarize our review findings to form an outlook on dCRISPR that will provide a guidance for its future development as the next generation of CRISPR-Dx.

2 CRISPR Associated (Cas) Proteins

Since the initial discovery of CRISPR-associated proteins, the landscape of the field has rapidly changed as newer variants are discovered and documented. It is critical to note that each of these different variations of Cas proteins exhibits unique features that separate them from their analogues [20, 21]. The most notable Cas proteins are classified as Class II CRISPR proteins that combine targeted binding with specific cleavage into a single complex [6]. Variations exist between Class II proteins in PAM [22], target preference [21, 23, 24], protein size, enzymatic rates [25], and optimal reagents [20, 26]. It is also important to note that variations occur between the same proteins derived from different sources. Thus, it remains vital for future CRISPR-detection systems to have access to a concise summary. **Figure 1** summarizes the differences between the most common examples of Cas 9 through 14 and provides design rules that are crucial to the development of CRISPR detection platforms.

2.1 Cas 9

A historical development in CRISPR systems was the discovery of Cas9. This protein was the first of CRISPR's Class II proteins that combined the multiple-protein functions of guide-RNA binding and target cleavage into one single protein (**Figure 1A**) [6, 27]. Therefore, this revolutionized gene-editing by drastically simplifying the use of a CRISPR system. Cas9 requires both a tracker RNA and a CRISPR RNA (crRNA) to satisfy its binding requirements [16]. In the presence of a target, the crRNA-guided Cas complex will bind to the dsDNA and cleave the nucleic acid strand. Subcategories of Cas9 range from 900 to more than 1600 amino acids in length, and its most common analog requires a specific 'NGG' protospacer adjacent motif (PAM) [28]. Overall, Cas9 remains a popular tool for gene editing despite its design complexities. In addition, diagnostic methods have been developed with Cas9 [29], but they have been rapidly phased out

for the simplicity of Cas12 and Cas13 systems (**Figure 1B&C**).

2.2 Cas12

When initially discovered, Cas12 was first conceptualized as a gene editing tool that would replace Cas9 [16]. It demonstrated RNA-guided DNA targeting with just the use of a crRNA, removing the need for a tracrRNA (**Figure 1B**). Similar to Cas9, Cas12 will cleave target ds/ssDNA, when bound to its complement crRNA and in the presence of the target. Not long after the discovery of Cas13's collateral cleavage activity, Cas12 was also found to demonstrate the similar phenomenon (**Figure 1B**), thus introducing its application toward CRISPR-Dx like Cas13 before it. While still used in labs for gene-editing, Cas12 has widely been adopted by molecular diagnostic labs due to its ability to partner with DNA from nucleic acid amplification [14]. Amplification methods remain the gold standard for molecular diagnostics and offer ultra-sensitive detection for infectious diseases. Since the development of *HOLMES* (one-HOur Low-cost Multipurpose highly Efficient System), many studies have implemented the use of Cas12 detection [11, 14, 30, 31]. These studies have shown Cas12's ability to detect amplicons from PCR, RT-PCR, LAMP or RT-LAMP for DNA or RNA detection, respectively. Thus, these studies demonstrate the potential of Cas12 for CRISPR-Dx methods that provide ultra-specific detection.

2.3 Cas13

The first protein discovered to show collateral cleavage activity of unbound nucleic acids was Cas13. Compared to Cas12, Cas13 is capable of RNA-guided RNA targeting. The mechanism between enzymes remains similar, but Cas13 is capable of targeting ssRNA rather than DNA. Guided by a crRNA specific to the target sequence, Cas13 will cleave ssRNA. The discovery of collateral cleavage created the field of CRISPR-Dx by simplifying the methods of detection using CRISPR systems [27]. Prior to the discovery of collateral cleavage, dCas9 was fluorescently tagged for detection [16]. Now nucleic acid reporters are added to Cas12 and Cas13 systems that carry a bound fluorophore and quencher. When bound to their specific target Cas12 and Cas13 will cleave the reporter and subsequently separate the fluorophore from the quencher. Thus, allowing the fluorescence of the bulk assay to signify the activity of the Cas protein. Like Cas12, Cas13 requires a single crRNA for target guidance [32]. LbCas13a has also demonstrated a smaller protospacer flanking region (PFS) than Cas12 or Cas9. **Figure 1C** shows that Cas13 only requires a 'Not G' nucleotide to flank its target sequence [12, 33].

2.4 Cas14

The most recent addition to CRISPR's toolbox is Cas14. As a much shorter protein than previous analogs, 400-700 amino acid length, Cas14 has been shown to be capable of RNA-guided ssDNA targeting without the need for a PAM sequence [34]. This enzyme requires both a tracrRNA and crRNA to help facilitate the capture of target ssDNA for cleavage. This novel protein presents simpler detection in a form factor half the size of most Cas12. Cas14 has a reported activity rate comparable to Cas12. (**Figure 1B&D**). The potential of Cas14 for CRISPR-Dx and dCRISPR remains to be seen, but it is encouraging to see the discovery of novel Class II proteins with unique characteristics compared to the initial versions (Cas 9-13).

3 Digital CRISPR Theory

3.1 Principles

CRISPR-Dx presents itself at the forefront of molecular diagnostics because of its sensitive and ultra-specific capabilities for single molecule detection. It has advantages over commonly used amplification methods. PCR requires long wait times and requires complex thermal systems to run properly. LAMP and RPA offer simplified isothermal amplification methods but are highly susceptible to false positives. CRISPR assays are simpler to operate than PCR, yet more specific than the top isothermal assays. CRISPR diagnostics offer highly specific detection through required binding and matching of three separate distinct regions. However, to achieve improvements over PCR and isothermal methods, CRISPR assays must demonstrate decreased testing times, reduced and constant temperatures, and increased sensitivity. While the majority of bulk CRISPR assays still lack these improvements, dCRISPR offers a rapidly growing segment of CRISPR-Dx that offers the most potential.

The workflow of dCRISPR parallels previous digital systems (**Figure 2A**). Systems start with an extracted sample that is then combined with the detection assay. These combined reagents and target are then distributed across numerous partitions. After the reaction time, the array of partitions can be imaged and classified for quantification (**Figure 2A**). Digital CRISPR boosts LOD performance, compared to bulk CRISPR assays, by decreasing the volume of the individual reaction and consequently increasing the minimum concentration for positive samples [18, 35]. Prior CRISPR assays were limited by bulk reactions and therefore required pre-amplification to

boost positive samples into a concentration range that CRISPR could detect. While preamplification does improve CRISPR, it presents issues for molecular diagnostics. Preamplification increases the length of time needed to run an assay, and it requires meticulous planning to combine with CRISPR assays. Thus, digitalization offers an alternative to CRISPR-coupled-preamplification since it reduces both the time requirement and complexity. Another benefit of digitalization is that systems are capable of absolute quantification. Poisson statistics define the concentration within the system and remove the dependence on a standard curve. Last, these systems include CRISPR's ultra-specific detection. Thus, dCRISPR presents a sensitive, simplified, rapid, ultra-specific, and quantitative method of molecular diagnostics. Factors that affect the performance of digital systems include error, partition size and number, assay efficiency, and the partitioning method.

3.2 Factors Affecting Digital Sensing Performance

3.2.1 Size of partition

As mentioned previously, the size of each partition will vary slightly. However, statistics and careful fabrication can minimize the error from volume uniformity. Poisson distribution is leveraged to calculate the concentration from empty partition numbers This is based on the probability of target concentration per partition and can be defined through Poisson probabilities. Basu *et al.* discusses the method and defines the target concentration as the following equation [36]:

$$C = -\ln(E)/V_d \quad (1)$$

Concentration, C, can be calculated from empty partition ratio, E, and volume of partition, V_d. Therefore, partition size directly impacts LOD (smallest concentration) and dynamic range (highest-lowest concentration) performance of digital systems [37]. Here we define LOD as the smallest concentration that can be detected against the background by a single positive well. In digital analysis the limit of quantification (LOQ) and LOD can be identical depending on the selected precision. By definition, LOD is defined as the smallest concentration that can be reliably detected against the background. LOQ is similar, it is defined as the smallest concentration that can be reliably detected with a predefined precision.

When we consider the extremes of equation 1, E approaches a maximum or minimum, this equation decomposes into two separate equations for LOD and UQL. S represents the partition

threshold that can be detected to differentiate between background signal and positive wells at low concentrations.

$$E = n_e/n \quad (2)$$

Where at lowest concentrations $n_e = n - S$, and at highest concentrations $n_e = S$. Then, at the lower and upper boundary concentrations:

$$C\ (LOD) = -\ln(\frac{n-S}{n})/V_d \quad (3)$$

$$C\ (UQL) = -\ln(\frac{S}{n})/V_d \quad (4)$$

These equations represent the concentrations for LOD and upper quantitative limit (UQL) respectively. The difference between these two metrics is defined as the dynamic range. We see in both equations that concentration and partition volume have an inverse relationship. Therefore, when designing a digital system targeting the best LOD, the volume of each partition should be as large as possible. On the other hand, when UQL or dynamic range is prioritized, the partition volume should be as small as possible. This compromise is demonstrated in **Figure 2B-D** where LOD performance can be seen to increase as partition volume increases. Consequently, **Figure 2C&D** show that both UQL and dynamic range decrease in magnitude as the partition volume increases.

Last, partition volume in coordination with the number of partitions defines the total amount of sample that can be processed. Example sample sizes are shown as contours in **Figure 2B-D** as products of the number of partitions and partition volume. As partition number and partition volume increase, sample capacity also increases. The input sample volume must be carefully considered as it will place operational limits on the digital system. As seen in **Figure 2B-D**, the sample size plotted as contour lines defines the region of obtainable LOD and dynamic range. It is well known that absolute quantification is constrained by partition volume and number, but their cross relationship remains even more important for sample size.

3.2.2 Number of partitions

Since absolute quantification of digital systems is defined by statistical methods, one may initially assume that the more partitions the better. From our theoretical plots in **Figure 2B** we see that this inference does make sense as LOD performance increases with larger partitions numbers. However, we see a minimal effect in UQL and dynamic range when the partition number is

increased (**Figure 2C&D**). These upper limit concentrations are dominated by the partition size rather than the partition number. There is a slight increase as partition number grows larger, but the overall trend in UQL (and dynamic range) is much more prominent along the partition volume axis (**Figure 2C&D**). To summarize, both LOD and dynamic range have proportional relationships with the partition number. LOD is affected more than dynamic range; however, both LOD and dynamic range are affected by other parameters. **Figure 2B-D** shows that partition number, partition volume, and sample size all have effects on the theoretical performance of digital systems. These must all be considered when designing a digital assay to accurately define an operating range of concentrations that enable absolute quantification. In summary, the combination of partition size, sample volume, and number of partitions define the theoretical LOD and dynamic range for dCRISPR systems. Consideration of these parameters and innovations to meet their desired requirements are critical for the next generation of dCRISPR platforms.

3.2.3 Partitioning method

The accumulation of all the previously mentioned factors occurs with the selection of a partitioning method. Partition size, number of partitions, and sources of error vary between partitioning technique. These methods differ in physical formation, but the effect of partition size, number, error, and efficiency is culminated through partitioning method. Digital droplets can be produced on an extremely large scale or in different batch sizes, but numerous droplets requires large sample volumes and time to generate the droplets [38]. Droplets must then also be carefully maintained, protected, and transferred to imaging systems. Microwells can introduce self-partitioning into microfluidic chips, but wells are not as numerous or flexible as droplet methods [18]. With innovative design, either method could be simplified for dCRISPR but the benefits and setbacks of each method should be measured before selecting the appropriate technique. Last, partitioning method is the final factor that must be carefully selected when designing a dCRISPR system, for it is the summation of all prior factors. In the following sections, we will discuss further the methods of partitioning used by dCRISPR systems.

3.2.4 Cas protein catalytic activity

The performance of a digital system can be affected by assay efficiency and assay velocity. First, efficiency can be broken down into two further categories, sensitivity, and specificity. Bulk CRISPR-Dx assays without preamplification have been shown to have limited sensitivity (pico-

to femtomolar ranges). Thus, introducing these assays into digital systems with reaction volumes of nano- or picoliters enables CRISPR detection within partitions. In partitions with CRISPR targets, the reduced volume creates micro-bulk assays with target concentrations that are detectable via CRISPR detection methods. For example, a 10 µL sample split across 10^7 partitions of requires partitions of 1 pL. If the initial sample concentration was originally 100 aM, there will be 600 target molecules spread across 10^7 partitions. Assuming each target is separated into its own partition, those positive partitions now contain a target concentration of 1.66 pM. On the other hand, CRISPR detection methods have been shown to exhibit extreme specificity in target binding and cleavage activity [9, 11-14, 20, 21, 26, 33]. Compared to isothermal amplification based digital assays, dCRISPR offers a highly specific digital assays that will have an extremely low probability of producing a false positive from a partition.

Second, the testing time of digital assays can be affected by assay velocity. Enzymes with faster reaction kinetics (K_{cat}) produce a detectable concentration in a shorter time. The concentration C can be represented as the catalytic activity rate (K_{cat}) multiplied by time (t) and divided by partition volume (V_d).

$$[C] = K_{cat} \cdot t/V_d \quad (5)$$

Therefore, this equation represents how an enzyme with higher K_{cat} will require a shorter reaction time to produce the same concentration as a slower enzyme. Coupled with digital partitioning, low target concentrations can be detected at similar times to higher concentrations. Thus, enzyme kinetic rate is a critical parameter to understand when designing a digital CRISPR system. Despite Cas proteins exhibiting a range of K_{cat} rates [25], dCRISPR assays have reduced their testing times to under 20 minutes [19]. The addition of amplification to CRISPR inside a digital system offers a boost to sensitivity that otherwise can be constrained through proper partition design. The extra time and CRISPR incompatibility of amplification add more complexity than benefit for digital assays [35]. Digital methods offer increased sensitivity and reduced time for CRISPR assays, two shortcomings that bulk amplification is only able to temporarily solve.

3.3 Sources of Error

Compared to bulk analysis, digital assays have far greater independence from detection systems and assay chemistry. Binary classification of digital partitions greatly reduces the associated error of digital systems from system readouts [36]. Errors can be mitigated through

background noise suppression and robust binary classification. However, digital methods still contain uncertainty from the partitioning process [18, 35]. To develop robust, repeatable, and relevant techniques, sources of error must be understood and acknowledged so that they can be minimized. At low concentrations subsampling error dominates the lowest detection limit, while partitioning error sets the upper detection limit at high concentrations. Both forms of error are dependent on the instrumentation used, while partitioning error may also include bias from the partitioning method and subsampling error itself.

An unavoidable source of error is human error. In many of the digital systems described, user error can manifest as loading error, handling error, or improper techniques that can affect all other sources of error. Human error can be minimized through robust engineering and process automation. The following sections will review these sources of error in detail, outline their methods and offer solutions to mitigate their effect.

3.3.1 Subsampling error

Errors from subsampling occur when digital assays do not analyze the entire volume of sample and when sample scattering occurs into partitions. This causes large variations between replicates and introduces an unavoidable source of error. Subsampling uncertainty can be modeled as the following equation:

$$u_s = z_c \sqrt{m}/m \quad (6)$$

where m is the expected number of targets in the sample and for a 95% confidence interval z_c should be 1.96 [36]. From this equation and **Figure 2E&F** we can see that subsampling error is most prominent at low target concentrations. The scarcity of target makes equal distribution between partitions difficult. Targets can be lost during sample preparation or while partitioning. Also, at low concentrations there is an increased chance for multiple targets to accumulate inside one partition. This causes issues when attempting to quantify at low concentrations. For example, when analyzing a sample with only 100 targets. It becomes difficult to accurately disperse all 100 targets into their own partitions when there are numerous partitions ($>10^5$). Several targets will be lost in processing, several could be placed within the same partition, and the effect on quantification due to these instances is defined as subsampling error. With only select positive partitions, each true positive well represents a larger percentage of all positive partitions than at higher concentrations. For this reason, endpoint analysis depends on proper displacement and

adequate partition numbers to ensure targets are displaced into a partition. On the other side, when *m* becomes very large, this type of uncertainty becomes minimal. In true testing scenarios when concentrations are unknown, it becomes imperative to properly design the operational limits for dCRISPR systems to minimize subsampling error.

3.3.2 Partitioning error

Partitioning errors occur because there is a variation in target distribution between separate digital trials. This variance occurs in the number of empty partitions and will then propagate to the calculated concentration of the bulk sample. Like subsampling error, partitioning error is based on a binomial process outlined by Dube *et al.* where the uncertainty is given by:

$$u_p = \frac{1}{\lambda}\ln\left(\frac{E+z_c\sigma_E}{E-z_c\sigma_E}\right) \quad (7)$$

$$\sigma_{E=\sqrt{E(1-E)/n}} \quad (8)$$

where E is the ratio of empty partitions to all partitions, λ represents the average number of targets per partition, σ_E is the standard deviation of negative partitions (E), and n is the total number of partitions [39]. Consequently, the uncertainty in measure concentration becomes significant at very high concentrations where the number of empty partitions approaches 0, and at very low concentrations where λ approaches 0 and E approaches 1. Then for each digital system there is a working range of concentrations that minimize the effect of partitioning error on the concentration readout (**Figure 2E**). However, partitioning error can also be minimized by increasing the overall number of partitions. As this happens the standard deviation between negative partitions will decrease and subsequently reduce the uncertainty. In **Figure 2F**, the uncertainty dips below 3% for a larger range of concentrations when one million partitions are used. Not all digital systems will be capable of arbitrarily increasing their partitions number, but it is a critical design note that partitioning error can be minimized in a system by using controlled partition numbers and understanding the target concentration range, λ.

3.3.3 Partition uniformity

Due to the nature of digitalization and absolute quantification, it is critical that the volume of partitions be accurately defined and controlled. A distribution in size is expected but must be normal for simplified absolute quantification. In fact, the Poisson model for quantification does not take into consideration volume variation. However, as Pinheiro *et al.* discusses, the uncertainty

can be minimized to under 1% by utilizing more than 10^5 partitions [40]. Thus, partition number has a similar relationship with volume-based errors as to dynamic range. These results signify that higher partition numbers can help to reduce error from volume variations. From the studies we sampled, there were multiple partitioning systems that contained more than Pinheiro *et al.'s* recommendation. These systems used droplet emulsion, droplet generators, and microchambers. While these studies did not quantify the error within their systems it is critical to understand the effect of volume distribution within a digital system. Therefore, partition methods that produce numerous and robust volumes should be used as a best practice to remove errors caused by volume non-uniformity [40, 41].

3.3.4 Single enzyme kinetic noise

Digital assays are traditionally immune to enzyme heterogeneity, where PCR and LAMP amplification create a strong, distinguishable signal through exponential growth. CRISPR diagnostics demonstrate linear reaction kinetics. Therefore, the endpoint analysis of digital CRISPR methods will have much lower signal to noise than digital amplification methods. As a result, enzyme activity can introduce large biases into sensing performance. Studies have explored enzymatic distributions and the effect on activity rate distribution [42], [35]but CRISPR Cas measurements are sparse beyond bulk measurements [25, 35]. For example, digital platforms partition samples into reactions on the order of pico-liter volumes. As partition number increases the probability that each pico-reaction has more than one Cas protein decreases. If we consider equation 5 and rearrange it to compare K_{cat} against time (t) the resulting equation 9 demonstrates the effect on sensing time.

$$t = {V_d \cdot [C]}/{K_{cat}} \quad (9)$$

When the K_{cat} for a given Cas has a distribution of values, that distribution will be inversely proportional to the time needed for detection purposes. In cases where the Cas has a large distribution in activity rate, wells with slow enzymatic activity could produce false negatives if the reaction time is not long enough [35]. On the other side, Cas enzymes with narrow activity distributions will demonstrate very specific time distributions where endpoint analysis should be conducted. Hence, enzyme kinetic distribution is a source of error that most works have not thoroughly studied. It remains a critical need of study to develop robust and rapid digital CRISPR platforms.

3.3.5 Sensor noise

Inside each digital system, quenched and unquenched fluorophores are excited and emit light in different amounts. This enables the identification of positive wells through unquenched fluorophores. However, when bound to quenchers, fluorophores are still capable of a limited amount of fluorescence. This generates background noise within readout systems that must be properly filtered out, or an error is introduced. At low concentrations, positive wells may exhibit lower levels of fluorescence. The electronic devices used in readout systems (optoelectronic and field effect transistors) will also have internal noise that will add error to the system. These sources of error are negligible at higher concentrations when the signal to noise ratio becomes very large. However, at low concentrations shot noise, flicker noise (1/f), and thermal noise can be significant. When background fluorescence and electronic noise cause similar intensities to true-positive wells, the LOD of the system can be compromised. The more false positives created from background fluorescence, the lower the performance of the digital system in terms of LOD. **Figure 2G** shows the relationship between false-positive partitions, *S*, and LOD. As the noise increases, LOD performance decreases. In digital systems, post-processing, binary classification, and robust optical setups can help minimize errors due to background noise.

Another key requirement of all digital systems is the proper segmentation of partitions. Improper separation can result in cross-contamination between partitions via target or fluorescent probe diffusion. This will cause improper partition classification and will affect the total output of the system. This would be considered a small section of partitioning error but can be eliminated by properly engineering digital systems with reliable separation.

3.3.6 Classification error

The most common method of eliminating error from background noise is to define a fluorescent threshold that defines a positive result. Numerous positive and negative wells should be tested to generate a clear division between the two samples in fluorescent output [35]. The threshold value should be set with statistical confidence to be separated from the mean and standard deviation of noise. The effect of error can be minimized through these developed methods. In **Figure 2H**, the distribution between high and low fluorescent wells can clearly be seen, but the defined threshold changes for each trial. Therefore, it is important to implement software measures to analyze and define specific thresholds for each trial and run of digital systems

[18, 43].

3.3.7 Summary

Overall, sources of error are present in every facet of digital detection from sample generation down to partition classification. Therefore, the development of any digital detection system must have a targeted approach that understands the balance between the sources of error we have outlined here. **Figure 2** provides theoretical guidelines for digital systems based on sample size, partition volume, number of partitions, and the sensing performance of the system (LOD and dynamic range). Beyond that, detection systems must be engineered well to segregate background noise from positive partitions and be coupled with robust software tools to classify the partitions correctly. Innovations in engineering will allow digital detection to become more robust, easier to use, and push dCRISPR forward as a detection platform.

4 Digital CRISPR Strategies

The current landscape of dCRISPR remains limited and scattered across several different concepts. To compare the performance of all dCRISPR systems, we created three subcategories or strategies to compare against real-life performance. Strategy 1 includes systems that hold the highest theoretical potential through isolated dCRISPR (**Figure 3A**). Next, Strategy 2 systems partition reactions, but include amplification (**Figure 3B**). Last, Strategy 3 includes systems that use CRISPR-Dx coupled with amplification in a two-stage setup (**Figure 3C**). Digital methods introduce a solution to increase the sensitivity of previous CRISPR assays and help disconnect CRISPR assays from amplification. The addition of amplification inside partitions has been shown to increase the LOD of systems but also doubles the entire testing time required. Similarly, external pre-amplification in a two-stage manner adds additional time and decreases the likelihood of automation by introducing numerous and complex sub-steps. Our review of all three strategies will compare the performance of partition method, LOD, dynamic range, and testing time to create an outlook for the future of dCRISPR systems.

4.1 Strategy 1: Amplification Free

Starting with Strategy 1, these systems include dCRISPR methods that only rely on CRISPR detection inside of numerous partitions for detection methods (**Figure 3A**). These introduce the

simplest form of dCRISPR that includes both the benefit of increased sensitivity and decreased time over bulk CRISPR assays. From our review there are six studies that can be classified as Strategy 1. These include both Cas12 and Cas13 studies and we found that all systems in this strategy use one of two partitioning techniques: droplet emulsion or microchambers.

4.1.1 Partitioning method

First, droplet partitioning remains one of the largest and most important subgroups of partitioning methods. In droplet-based systems, micro droplets are formed inside an immiscible fluid by a variety of techniques. These methods include emulsification and fluid shear force valves for the discrete formation of droplets. The advantages of droplet-based techniques include rapid and numerous formations of micro-partitions but are known to be less precise and controllable than other methods. Droplets are stored within an immiscible fluid and spread thinly over a larger area to be imaged [38, 44, 45].

Microfluidic valves allow for robust and continuous control of droplet formation inside a microchannel. **Figure 4A** shows crossflow valves that introduce the reaction solution perpendicularly to the immiscible fluid [46]. Thus, by altering the angle of approach between the two liquids and the velocity of flow, the droplet size can be manipulated [38]. Second, co-flow channels introduce the two fluids together in a parallel arrangement (**Figure 4B**) [44]. Last, the *Ultralocalized Cas13* system and Yue *et al.* used flow-focusing systems to introduce the reaction solution into a pinch-point between two channels of immiscible fluid (**Figure 4C**) [45, 47-49]. By adjusting the geometry, flow parameters, and immiscible fluid these systems can vary the size of droplets produced.

For larger bulk emulsions, vortex techniques are easy to adopt as the combination of the reaction solution and immiscible fluid inside a container can form droplets when vortexed rapidly for a defined amount of time (**Figure 4D**). While convenient and simple, vortex emulsification requires additional steps for imaging the partitions [18].

Second, advances in micro-machining and lithography have produced microfluidic systems capable of partitioning into microchambers. These methods often offer simpler methods with more repeatable volumes. However, the number of partitions is defined by the size of the chip and manufacturing techniques. Also, microfluidic chips fabricated with these methods take longer to produce than many droplet techniques.

The most common form of microchamber partitioning is accomplished using microfluidic chips that are capable of self-partitioning. In this manner the intricacies of partitioning are engineered into the microfluidic channels of the chip. The reaction solution can be inserted or dropped on the chip and through pressure manipulation or centrifugal force the reaction solution is dispersed properly to the appropriate microchambers. For example, Yu *et al.* uses polydimethylsiloxane (PDMS), a popular material for this style of microfluidic chip because microwells can be created via lithography to collect reagents as they are pushed through the chip [50]. Top-down wells, illustrated in **Figure 4E**, self-partition when the reagents are driven over top of microwells. The reagent fills the microchambers from the "top-down" as it continues through the chip and creates numerous uniform wells. Other forms of PDMS digital chips include vacuum PDMS and PDMS pumps that take advantage of the high deformability and gas permeability of the material [18]. Last, other chips of varying material such as poly (methyl methacrylate) (PMMA) or other plastics can be created but require outside manipulation. Shinoda *et al.* uses both polycarbonate and glass in separate studies to create microchamber arrays [51, 52]. In these cases, an external pump, syringe, or pipette is required to assist in the fluid insertion. These chips tend to be easier to manufacture and operate in hand; however, they are limited in the size and capacity compared to PDMS and lithography techniques.

4.1.2 Performance

Across the board, Strategy 1 systems have a much wider range of performance metrics than Strategy 2 or 3 systems. The claimed LOD of strategy 1 systems range from 2.4 – 9300 aM with a mean of 2392 aM. Dynamic range was reviewed and collected as a numeric fold increase in magnitude from the LOD to the highest tested concentration of the system. Strategy 1 systems demonstrated a range from 1 – 6-fold increases over their respective LODs with a mean increase of 4.2. The average time of testing for these systems was just over 32 minutes with the longest and shortest tests using 60 and 5 minutes, respectively. If we utilize the figure of merit presented in our previous work [19], Strategy 1 systems demonstrate a range of values from 21.6 to 225,000 (aM•min) listed in **Table 1**. Based on these results, the *opn-SATORI* system demonstrated the highest performance with the lowest FOM. In particular, *opn-SATORI* used a 0.03 pL microchamber array containing 10^8 partitions and accomplished a LOD of 2.4 aM in under 9 minutes [51].

4.1.3 Multiple crRNA

There are two studies that studied the effects of addition crRNA on detection limits. They use identical partitioning methods to their parent studies such as droplet emulsion and microchambers. However, they showed an increase in sensitivity and improved the LOD by 38 and 80 percent respectively over their parent setup [52, 53]. Both setups are tested within 15 minutes and demonstrate LODs below 10 fM. Thus, their performance summarizes well in the calculation of FOM. The addition of multiple crRNA increased the performance of Son *et al.'s* system to second best within Strategy 1.

4.2 Strategy 2: In-partition amplification

Next, Strategy 2 systems combine nucleic acid amplification and CRISPR assays together in each partition (**Figure 3B**). These methods increase the complexity of systems as the chemistry between both assays must be optimized to work. Amplification assays in this strategy include either LAMP or RPA to target SARS-CoV-2 or *Human Papilloma Virus*. Many systems use Cas12 detection; however, the *MEDICA* system demonstrates HPV detection using RT-RPA and Cas13 [49]. In Strategy 2, we are introduced to several new partitioning methods: droplet microvalves, commercialized chips, and slip chips.

4.2.1 Partitioning method

First, methods of this strategy use another variation of droplet partitioning that uses microfluid shear forces to control the formation of droplets. Engineered geometries act as fluid valves that assist in the finite creation of droplets. These droplets are then collected in a basin at the end of the microfluid setup and later imaged. Like other droplet methods, a two-step process is required to first fabricate the droplets, then transfer them to an imaging stage [38, 45, 46].

Second, commercialized chips offer a simple partitioning method that only requires the assay of interest to be pipetted inside. Some chips only interface with their partnering digital readout system such as the Clarity digital chip (JN Medsys). The actual internals of the chip are unknown but it claims to have 1,600 pL partition volume with 10,000 partitions per reaction [54]. On the other hand, there are chips that can be used with external readout systems for detection. For example, the QuantStudio™ 3D Digital PCR 20K Chip (ThermoFisher Scientific) contains 20,000 microwells that can be filled by dropping the solution onto the top of the chip [55]. The chip requires a special seal, but then can be imaged with a fluorescent microscope. Overall, these chips

do not use specialized techniques to partition reactions; instead, these chips simplify the user process and reduce fabrication errors.

Third, slip chips are a method of microfluidic chip partitioning that segregates the reaction solution via a "slipping" motion of two planes passing over one another in very close contact [56]. This style of digital microfluidic chip does not require an external power supply or pump and can easily be manipulated by hand [57, 58]. Some studies have converted this style of chip to work with centrifugal forces to improve throughput volume. However, the unique partitioning method of slip chips remains limited for further integration and upscaling. Yu *et al.* uses a slip chip to first partition their CRISPR and RT-LAMP assays separately. Then in a secondary step after amplification, the "slipping" motion (seen in **Figure 4F**), combines the two assays together to begin the dCRISPR detection [59]. Slip chips offer a simple method of partitioning yet lack the large amounts of partitions that other formats can generate.

4.2.2 Performance

On average, Strategy 2 systems demonstrate the lowest LOD of all strategies but require a longer amount of time compared to Strategy 1. These systems have an average LOD of 6.98 aM and values ranging from 1 to 33 aM (**Table 1**). The dynamic range of strategy 2 systems showed an average 4.4-fold increase, but the time requirement increased to an average of 63.6 min. However, Liu *et al.* was able to demonstrate the fastest strategy 2 system with their *MEDICA* setup in under 25 minutes [49]. Overall, the *deCOViD* system demonstrated a FOM of 48 (aM•min), with the best performance in strategy 2. In detail, *deCOViD* is capable of detection down to 1.6 aM, an upper limit 4-fold higher than LOD, and testing within 30 minutes [60].

4.3 Strategy 3: Two-stage amplification

Last, one dCRISPR study performed amplification separate from the CRISPR assay and combined the reactions together using pico-injection. This method created partitions using a microfluid droplet generator and picoinjector to create an amplified dCRISPR system in a two-stage process. This study was capable of *Salmonella typhimurium* detection with Cas12. Wu et. al demonstrated a LOD as low as 3000 aM with an upper limit 3-fold higher. *DropCRISPR* requires 80 minutes and consequently produced the poorest FOM performance of all the studies sampled [61].

4.3.1 Partitioning method

The *DropCRISPR* system uses a microfluidic droplet generator that also includes a picoinjector (**Figure 3C**). The droplet generator was created using PDMS and patterned using soft lithography. In addition, the picoinjector was also fabricated from PDMS but required micro-3D printing to create the necessary negative mold [61]. Once bonded together, the droplet generator and picoinjector we also bonded to a glass slide. The system contained multiple inlet ports where the LAMP assay, oil, and later the CRISPR assay could be injected. Once the finalized CRISPR droplets were formed they were collected into a separate tube. Then, the CRISPR droplets were pipetted into an imaging chamber [61].

4.3.2 Performance

The performance of *DropCRISPR* platform lagged behind all other systems when ranked using the CRISPR FOM metric [19, 61]. They reached a LOD of 3000 aM with a detection time of 80 minutes. Their upper limit of detection was 3-fold higher than their LOD. The increased testing time is due to their unique partitioning method, yet this technique created 7×10^5 droplets of 33 pL volume. Droplet size and volume were similar to other well-performing systems, such as *MEDICA* [48, 49, 53]. Nonetheless, *DropCRISPR* demonstrated the highest FOM with 240,000 (aM•min).

4.4 Strategy benchmarking

All three strategies demonstrated similar dynamic ranges with magnitudes increasing up to 4-fold higher than the LOD. On average, strategy 2 systems demonstrated lower FOMs seen in Figure 5A, driven by lower LODs. At this time, amplification coupled dCRISPR systems are still more sensitive than systems that remove it (Table **1** and Figure 5B). Despite the large distribution in dCRISPR systems without amplification, these methods show the lowest FOM across all strategies. The field of dCRISPR remains broadly distributed. For the future of dCRISPR to succeed, targeted approaches in partition style, size, number, and engineering systems need to occur. Consequently, strategy 2 systems take two times as long to run than strategy 1 systems. Both strategy 1 and 2 showed similar partitioning methods between droplet formation and microchamber manufacturing. In addition, several strategy 2 systems chose to use commercial partitioning chips. Strategy 1 systems were equally distributed between flow-focusing systems and microchamber chips (Table 1).

Overall, the best performance across all strategies was seen in the *opn-SATORI* system with a FOM of 21.6 (aM•min). Son et al.'s Cas13 system, with multiple crRNAs, was not far behind with an FOM of 24 (aM•min), and even demonstrated a slightly better LOD of 1.6 aM. These systems used more than 105 partitions with volumes of 0.03 and 10 picoliters respectively [51, 53]. Both systems were classified as Strategy 1 dCRISPR setups, and so, we continue to envision that the future of dCRISPR systems lie in Strategy 1 setups as they offer the most potential for increased performance. While these systems remain broadly distributed in FOM (Figure 5A), we offer the topics discussed throughout our review to improve novel dCRISPR platforms.

5 Outlook and Perspective

5.1 Boosting dCRISPR LOD and dynamic range

Theoretically, dCRISPR needs to achieve a LOD close to 0.16 aM (0.1 cp/μL) to compare against the most sensitive molecular detection platforms. The lowest dCRISPR methods still fall short at around 1 aM with amplification still being used [54, 60, 62]. Without amplification, Shinoda et al. and Son et al. demonstrate the lowest LODs of 2.4 aM and 1.6 aM respectively [52, 53]. Even so, there remains an order of magnitude separation from amplification methods to dCRISPR methods that must be improved. From a methods standpoint, the answer is to increase the number of partitions without reducing the volume. The methods we have sampled here show how dCRISPR has an application for molecular detection. For further optimization, dCRISPR systems need to be pushed beyond 1 aM and accommodations for larger sample sizes (> 10 uL), larger partition volumes (102-104 pL), and numerous partitions (103-106) will be required. These benefits will allow for dCRISPR systems to be developed specifically targeting situational parameters. There exists a compromise between LOD and dynamic range, and improvements to either are not one-size fits all. We envision that strategic targeting of partition number and volume will allow for the development of dCRISPR systems with accurate LOD and dynamic range appropriate for their sensing application.

On the other hand, dynamic range can be customized by selecting an appropriate partitioning method. This will adversely affect LOD but can help for customized applications where large variations in sample concentration must be quantified. As an example, platforms performing viral load testing of HIV patients for dosed antiretroviral treatment would care more about high

concentration quantification than LOD. A large dynamic range ensures that the quantitative performance of the system will not be compromised at high concentrations. At maximum concentrations, digital assays plateau, lose quantification ability, and will require repeated testing and additional processing. The limit of detection improves as partition volume and number increase. In contrast, dynamic range improves for decreased partition volumes. Meaning that LOD and dynamic range have an opposite but proportional relationship to partition volume. Thus, a compromise must be made between LOD and dynamic range when designing partition methods. It is possible with digital systems to implement external strategies to improve dynamic range. Multiplex testing can help achieve higher dynamic range without limiting the sensitivity of single batch runs. Another solution is sample dilution. In this method, high sample concentrations are preemptively diluted to match the inherit dynamic range of the digital system. While this does not boost the true dynamic range of the digital assay it can help expand the range of the entire testing system and therefore boost performance. Improvements to dynamic range will help in handling larger sample volumes, maintaining quantitative ability, and eliminating quantification errors. Engineered systems that utilize any of these methods could provide improvements over the current field of dCRISPR assays. Thus, pushing dCRISPR toward more widespread use.

5.2 Novel Cas protein exploration

Recent studies have presented novel proteins such as Cas14 that present unique attributes over previously known proteins [34]. While we do present Cas14 in this review paper, at the time of writing there are no dCRISPR assays utilizing Cas14. Thus, the discovery and application of more novel proteins has the potential to increase the performance of dCRISPR systems beyond Cas12 and Cas13. Cas14 simplifies the capabilities of CRISPR DNases and introduces an enzyme much shorter than Cas12. Advantages to dCRISPR platforms are not directly apparent but its discovery leads well for the investigation of more novel proteins that may exhibit higher kinetic activity, more specific targeting approaches, unique cleavage activity, and unknown benefits to gene editing and CRISPR-Dx.

Digital CRISPR presents a method for further development and characterization of new and known Cas proteins. Discrete partitioning allows for single molecule characterization rather than relying on Michaelis-Menten kinetics from bulk assays. Therefore, the development, characterization, and discovery of novel CRISPR proteins can be precisely monitored [18, 35]. The

same methods can be applied to known Cas proteins such as Cas12 and Cas13 to better understand their kinetics and improve applications.

Last, several studies have explored using CRISPR's unique specificity and preferential cleavage to detect multiple targets [9, 30, 63, 64]. These studies use multiple crRNAs partnered with multiple Cas proteins to accomplish targeted cleavage of reporters bearing various fluorophores [64]. At this point, the use of multiplexed testing with dCRISPR has yet to be seen. Digital systems would have the ability to detect these upcoming technologies, but we expect assay performance, intensity thresholding, quantification, and subsampling error will be large areas of development for platforms that adopt multiplexed dCRISPR [9].

5.3 System engineering

Most of the dCRISPR methods reviewed in this work remain laboratory restricted. There remains a need for automated systems with the specificity of CRISPR and increased sensitivity . Including sample preparation steps will boost the capability of dCRISPR for areas of low resource. Current methods lack easier partitioning methods that can increase each partition's volume and increase the number of partitions by orders of magnitude. Coupling these improvements with portable imaging systems offers the most potential for applications.

The dCRISPR methods we present here translate very well for laboratory improvements. Improvements to partition volume and number will also increase sensitivity levels. In fact, reduced testing time from Strategy 1 dCRISPR platforms offers the most potential in laboratory settings. Rapid and quantitative NAT methods could alleviate the testing backlogs caused by other amplification-based methods when demand is high. Many of the systems we describe here use a high-end microscope with post-processing software for quantification. This will remain the most common setup out of dCRISPR systems until large innovations are made in user reliability, ease of access, portability, and sensitivity that allow these methods to be manufactured as commercial platforms for labs or settings beyond.

On the other hand, one study demonstrated that dCRISPR could be operated using a smartphone [50]. While their methods were limited, improvements in camera technology over the last two decades have made these improvements possible. Smartphones combine high-speed processing with high-quality onboard cameras, giving many people two essential tools to run digital readouts. Yue *et. al.* is the first to show dCRISPR detection on a smartphone platform, but

others have already demonstrated the capability for digital PCR and digital LAMP [65, 66]. As dCRISPR assays improve, we expect smartphones and dedicated software to become even more popular as methods to mobilize digital platforms.

The benefits of digitalization have been realized by many nucleic acid amplification tests (NAAT) that are applying their methods to interface with digital systems. There are numerous digital NAAT (dNAAT) methods that offer quantitative methods,increased sensitivity, and high accuracy [18, 65, 66]. Issues that plague dNAAT also restrict dCRISPR applications. For instance, microfluidic partitioning chips remain expensive to manufacture, partitioning methods are segregated from sample preparation, and droplet-based techniques offer little customization to partition volume and number [18]. Innovations are needed to simplify and integrate partitioning methods and sample preparation.

One method with potential to simplify digital partitioning is membrane absorption. This uses a porous material as an absorption media for digital detection [67]. These include porous papers, filtration membranes, or segregated membranes with intrinsic microchambers for trapping reagents. While similar to commercial chips, membranes offer much simpler manufacturing techniques. This helps reduce the price of systems and improves system wide integration. These porous materials are easy to obtain, store, and could be integrated with microfluidic chips to improve filling and automation techniques. Methods using LAMP have been demonstrated [67], and we envision that membrane digitalization has potential for future dCRISPR systems as the field expands.

5.4 Outlook

Overall, digital CRISPR stands as a powerful detection platform with the potential to lead the next generation of biosensing. Innovations are needed to simplify and integrate partitioning methods for improved LOD and dynamic range. These improvements lie within adjustments to partitioning method, volume, and number. All key parameters that define the sensitivity of digital platforms. Engineered systems that tackle these challenges offer significant benefits to the field of molecular detection, enzyme characterization, point-of-care testing, and nucleic acid testing. Complete systems improve upon the current NAT standards by inheriting the benefits of CRISPR: ultra-specific detection, reduced wait-times, and isothermal operation while also adding the benefits of digital methods: absolute quantification, decreased LOD, and increased dynamic

ranges. Laboratories would benefit from decreased testing times, while point-of-care systems can take advantage of simple yet quantitative NATs. Thus, the future of CRISPR-Dx lies with high performance dCRISPR systems integrated into complete engineering and clinical tools. A combination that will enable dCRISPR to compete efficiently with dNAAT for the next generation of biosensing.

Author Information

Corresponding Author

* Email: Weihua Guan (wzg111@psu.edu)

Declaration of competing interest

The authors declare that they have no known competing financial interests or personal relationships that could have appeared to influence the work reported in this paper.

Acknowledgments

This work was supported by the National Institutes of Health (R61AI147419) and National Science Foundation (1902503, 1912410, 2045169). Any opinions, findings, and conclusions or recommendations expressed in this work are those of the authors and do not necessarily reflect the views of the National Science Foundation and National Institutes of Health.

Figures and Captions

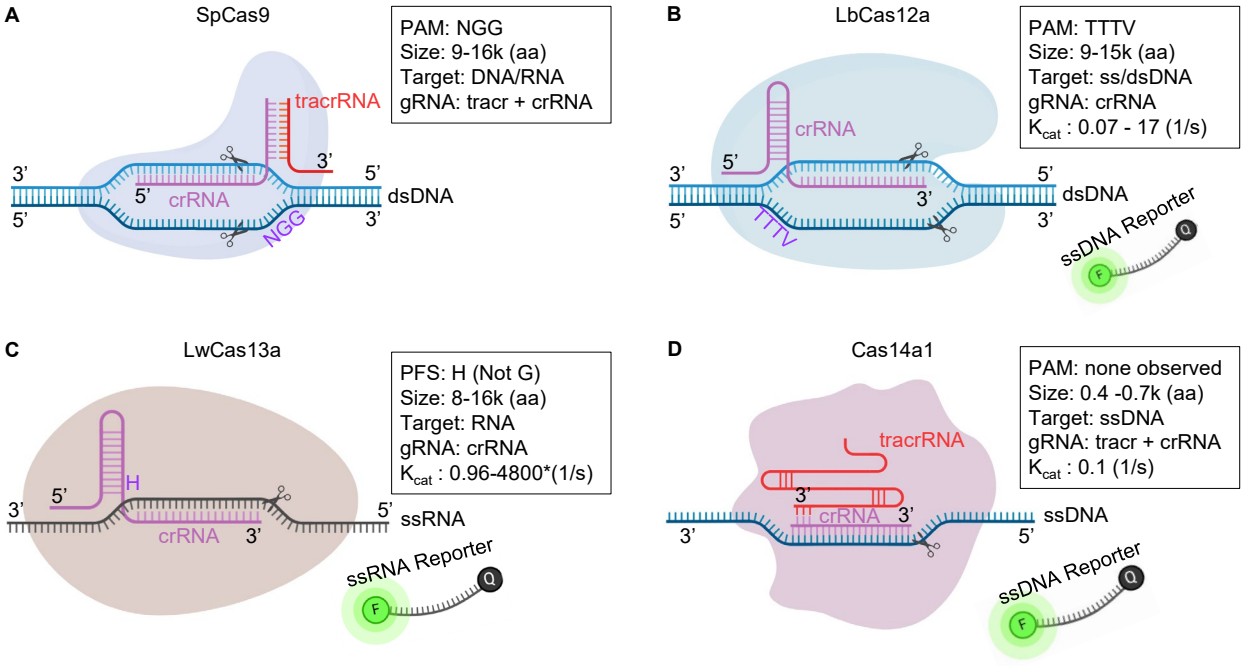

Figure 1. Variations between CRISPR proteins. (A) Cas9 requires both a tracrRNA and crRNA to satisfy its gRNA binding domain, can target DNA (ss or ds) or RNA, and has a NGG PAM in many variants. (B) LbCas12 is a similar sized protein to Cas9, however it only requires a crRNA to target ss/dsDNA. It requires a TTTA PAM and has been shown to demonstrate collateral cleavage. Catalytic activity rate (kcat) for Cas12 ranges from 0.07-17 (1/s). (C) LwCas13 is a crRNA guided RNA nuclease with a Not-G PFS. Recorded Kcat values for Cas13 range from 0.955-4800 (1/s). (D) Cas14 requires no PAM and exhibits collateral cleavage for ssDNA targets. [25] Note: Proteins derived from different sources will have variations from what are listed here. We have chosen to highlight the most common analogs for diagnosis. *Upper limit of 4800 cuts/s for LwCas13a has been reported by Shan et. al. [68], but has been challenged by Ramachandran & Santiago and does not match the theoretical calculation of Diego et. al. [25, 69].

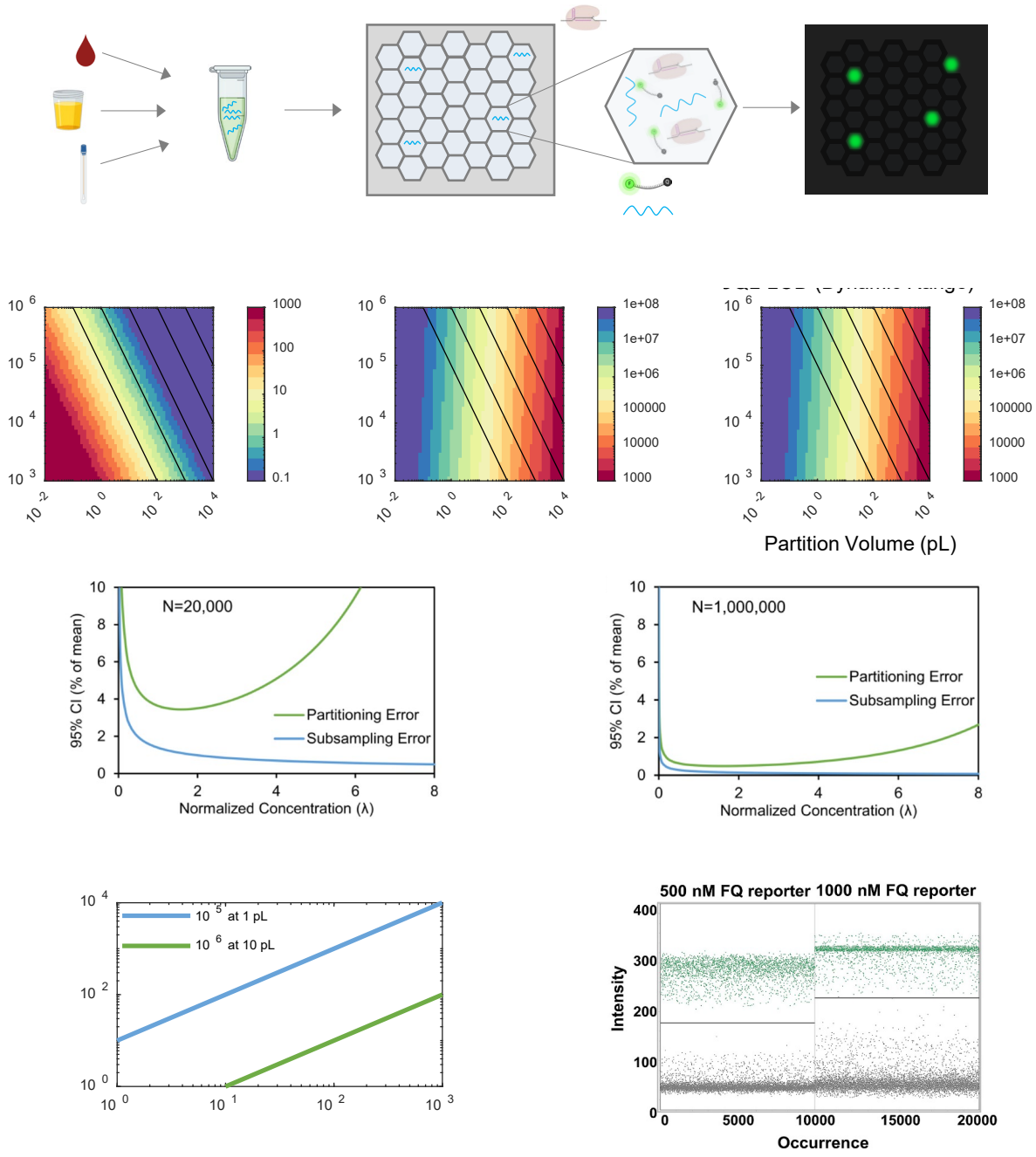

Figure 2. Workflow and factors that affect dCRISPR systems. (A) Samples are extracted, combined with the dCRISPR assay, and partitioned into numerous droplets or wells. These micro-CRISPR reactions create binary signals for quantification. (B) LOD distribution for different partition volumes and numbers. Contour lines map the constant sample volumes from partition volume and number combination. (C) Distribution of Upper Quantitative Limit for digital systems with varying partition volume and number. (D) Difference between the UQL and LOD to produce effective dynamic range of digital systems with varying partition volume and number. (E)

Normalized concentration (sample over total volume) vs uncertainty for partitioning and subsampling error at 20,000 partitions. Image from: [36] (F) Normalized concentration (sample over total volume) vs uncertainty for partitioning and subsampling error at 100,000 partitions. Image from: [36] (G) Simulated background noise vs LOD at two different digital setups: 10^5 partitions with 1 pL volume each or 10^6 partitions with 10 pL volume. Both setups lose LOD performance as background noise increases (H) Fluorescent Intensity of numerous positive and negative wells at two different reporter concentrations. The threshold that separates the software classification changes between assays. Image from: [49]

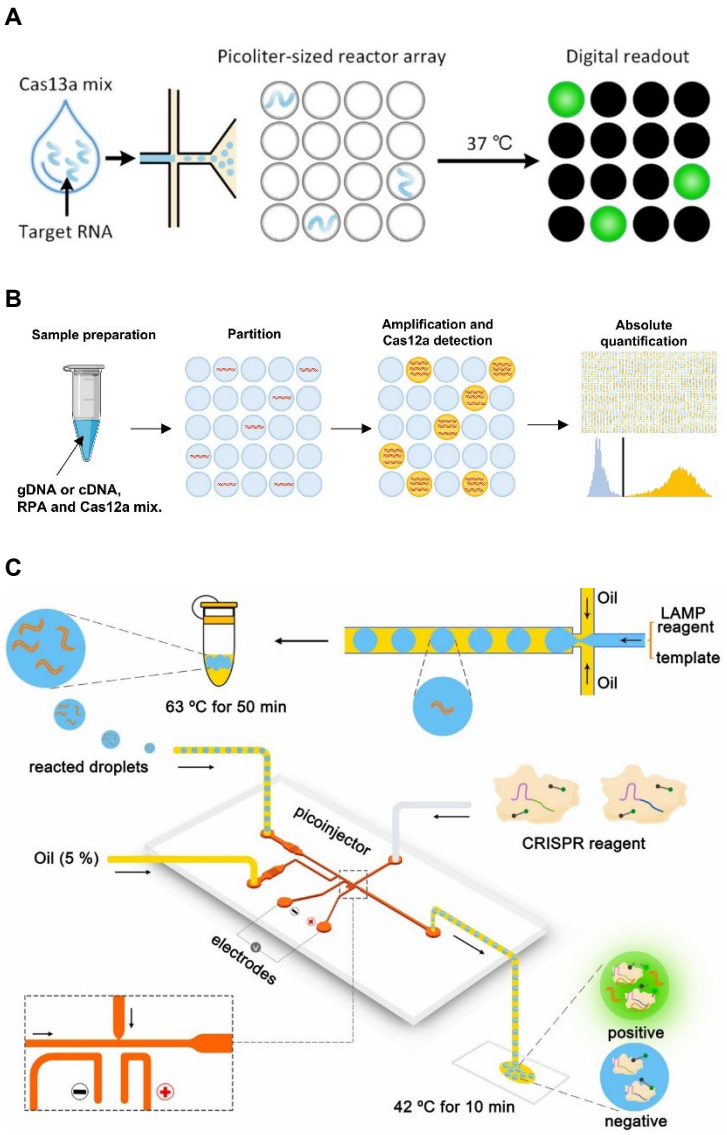

Figure 3. Detection principles and strategies for different dCRISPR systems. (A) Strategy 1 systems partition the CRISPR reaction, maintain temperature, and then image the array of partitions. Image from: [47] (B) Strategy 2 digital CRISPR systems partition a combined amplification and CRISPR reaction, maintain temperature(s) to amplify the target and then detect the fluorescence from the digital array. Image from: [62] (C) Strategy 3 systems partition an amplification reaction first. Then, systems introduce CRISPR reagents into each partition and image the secondary reaction. Image from: [62]

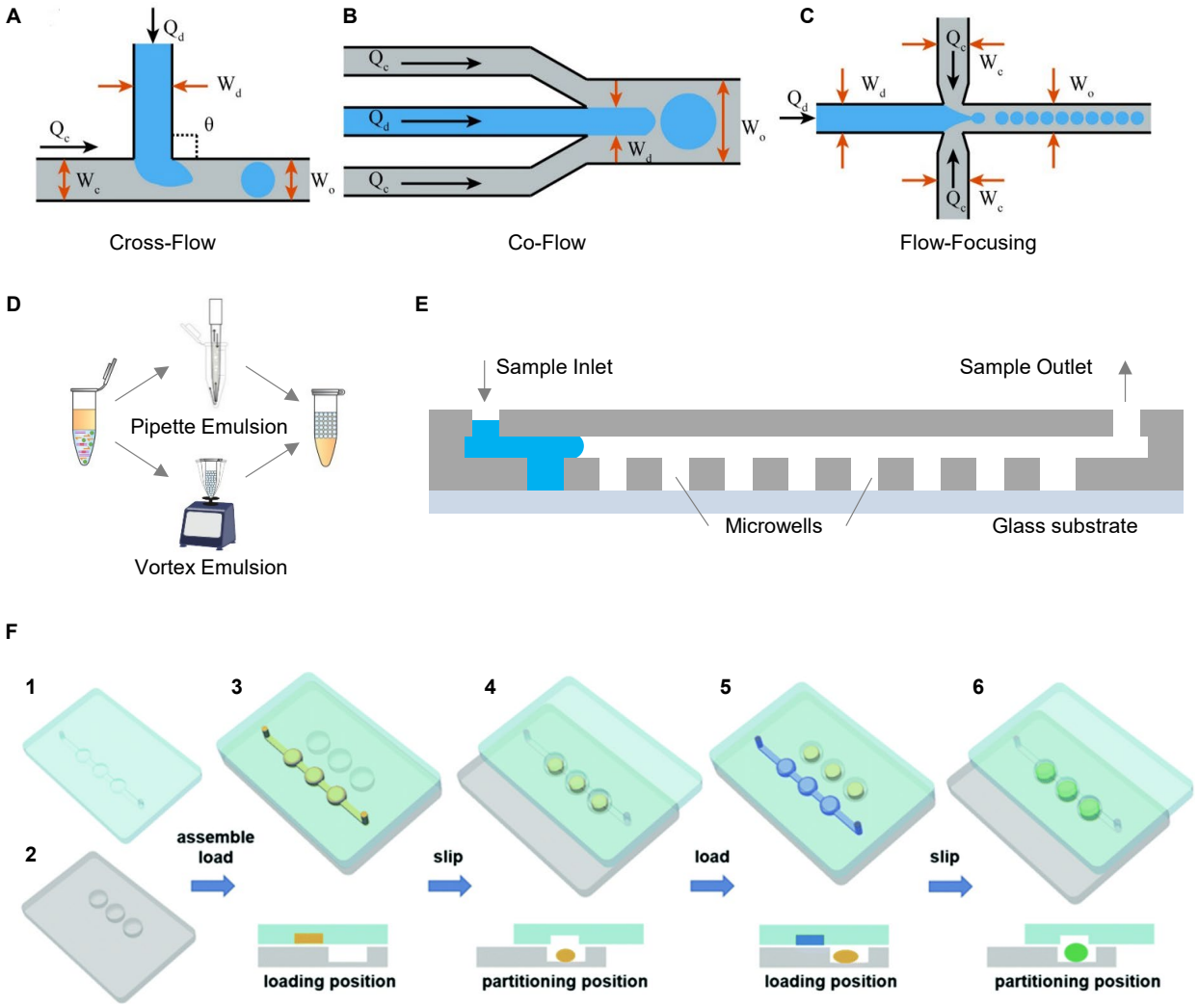

Figure 4. Partitioning methods for digital CRISPR systems. (A) Cross flow microfluidic channels create droplets from perpendicular intersections. Image from: [18] B) Co-flow microchannels introduce reagents alongside two parallel channels of an immiscible fluid. Image from: [18] (C) Flow-focusing microfluidic channels force the reagent between two perpendicular streams of immiscible fluid. Image from: [18] (D) Pipette mixing, vortex stirring, or even manual shaking can create small reagent droplets through emulsion. Some images from: [53, 70] (E) Microwells help self-partition when reagents are pumped or pushed through microfluidic cartridges. (F) Slip chips partition and combined reagents through close-contact translation between microfluidic layers. Image from: [59]

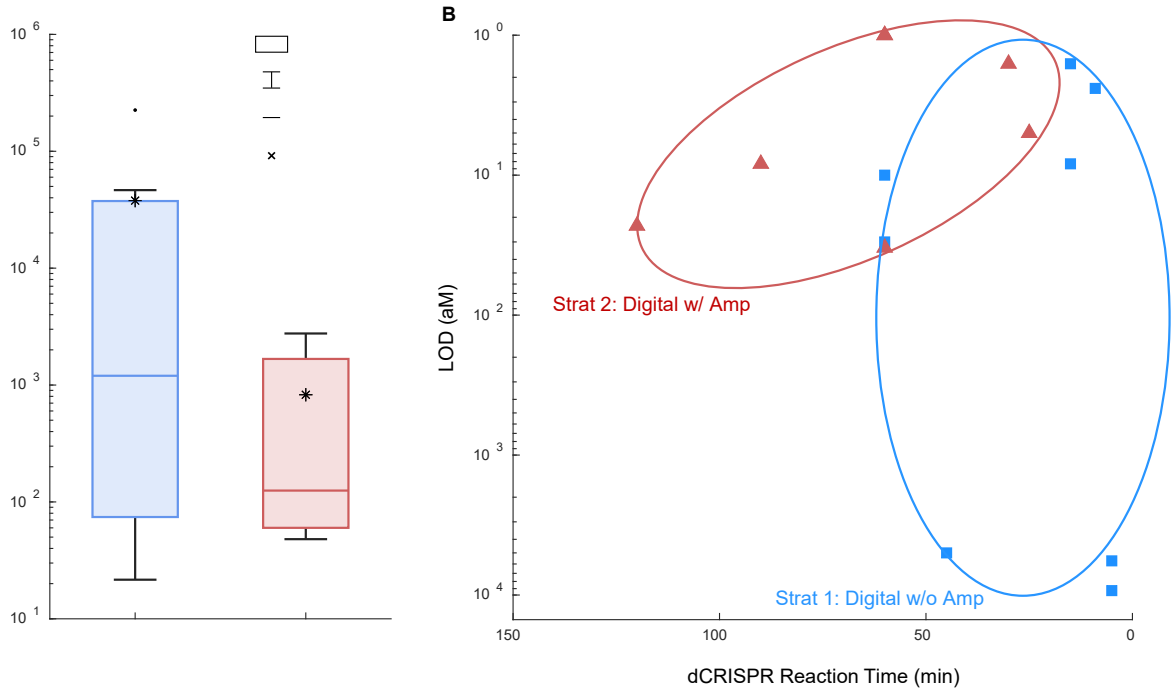

Figure 5. Digital CRISPR performance. (A) Distribution of FOM values for Strategy 1 dCRISPR systems and Strategy 2 dCRISPR systems. Mean values fall at approximately 38k and 800 (aM•min) for Strat 1 and 2, respectively. (B) Strategy 1 and 2 system performance plotted as reaction time vs LOD. Strategy 1 systems remain contained between 0-60 min but have large range of LODs. Strategy 2 systems remain contained from 1-100 aM LOD but have large range in reaction time.

Table 1. Summary of the reported digital CRISPR systems.

Pathogen	Target	Effector	Readout	Amplification	Partitioning Method	Number of Partitions	Volume of Partition (pL)	LOD (aM)	Dynamic Range (fold)	Total Time Req (min)	FOM (aM*min.)	Ref.
Strategy 1:	**Digital w/o Amp**						**Average:**	**2506.54**	**4.14**	**29.86**	**8178.35**	
HBV & HPV	DNA	LbaCas12a	Fluorescence	—	microwells	—	10	5000	1	45	225000	48
SARS-CoV-2	RNA	LwaCas13a	Fluorescence	—	microwells	1.00E+06	0.003	9300	4	5	46500	50
ASFV, EBV, & HBV	DNA	LbCas12a	Fluorescence	—	emulsion	1.00E+05	4.19	30	4	60	1800	46
SARS-CoV-2	RNA and microRNA	LbuCas13a	Fluorescence	—	emulsion	1.00E+05	1500	10	6	60	600	45
SARS-CoV-2	RNA	LbuCas13a	Fluorescence	—	emulsion	4.78E+02	10	8.3	4	15	124.5	51
SARS-CoV-2	RNA	LtrCas13a	Fluorescence	—	microwells	1.00E+08	0.03	2.4	6	9	21.6	49
Digital w/o Amp + multiple crRNA					microwells							
SARS-CoV-2	RNA	LwaCas13a	Fluorescence	—	microwells	1.00E+06	0.003	5700	4	5	28500	50
SARS-CoV-2	RNA	LbuCas13a	Fluorescence	—	emulsion	1.60E+05	10	1.6	4	15	24	51
Strategy 2:	**Digital w/ Amp**						**Average:**	**10.41**	**4.43**	**63.57**	**825.71**	
SARS-CoV-2	RNA	AapCas12b	Fluorescence	RT-LAMP	emulsion	1.50E+03	268	23	4	120	2760	44
SARS-CoV-2	RNA	Cas12a	Fluorescence	RT-LAMP	Slip Chip	2.40E+03	3200	33	4	60	1980	56
SARS-CoV-2	RNA	LbaCas12a	Fluorescence	RT-DAMP/LAMP	Commercial Chip	2.00E+04	700	8.3	6	90	747	
HPV	RNA	LwaCas13a	Fluorescence	RT-RPA	emulsion	1.40E+06	14.1	5	5	25	125	47
SARS-CoV-2	RNA	LbaCas12a	Fluorescence	RT-RPA	Clarity digital chip	1.00E+04	1300	1	4	60	60	59
SARS-CoV-2	DNA	AapCas12b	Fluorescence	RT-LAMP	Clarity digital chip	1.00E+04	1300	1	4	60	60	52
SARS-CoV-2	RNA	LbCas12a	Fluorescence	RT-RPA	Commercial Chip	2.00E+04	700	1.6	4	30	48	57
Strategy 3:	**Digital w/ Pre-Amp**											
Salmonella typhimurium (St)	DNA	Cas12a	Fluorescence	LAMP	droplet	7.00E+05	33	3000	3	80	240000	58

References

[1]J. E. Schmitz, C. W. Stratton, D. H. Persing, and Y.-W. Tang, "Forty Years of Molecular Diagnostics for Infectious Diseases," *Journal of Clinical Microbiology,* pp. e02446-21, 2022.

[2]Y. Zhao, F. Chen, Q. Li, L. Wang, and C. Fan, "Isothermal amplification of nucleic acids," *Chemical reviews,* vol. 115, no. 22, pp. 12491-12545, 2015.

[3]R. Pu *et al.*, "The screening value of RT-LAMP and RT-PCR in the diagnosis of COVID-19: systematic review and meta-analysis," *Journal of virological methods,* vol. 300, p. 114392, 2022.

[4]C. Uribe-Alvarez, Q. Lam, D. A. Baldwin, and J. Chernoff, "Low saliva pH can yield false positives results in simple RT-LAMP-based SARS-CoV-2 diagnostic tests," *PloS one,* vol. 16, no. 5, p. e0250202, 2021.

[5]P. Hardinge and J. A. H. Murray, "Lack of specificity associated with using molecular beacons in loop mediated amplification assays," *BMC biotechnology,* vol. 19, no. 1, pp. 1-15, 2019.

[6]R. Barrangou and P. Horvath, "A decade of discovery: CRISPR functions and applications," *Nature microbiology,* vol. 2, no. 7, pp. 1-9, 2017.

[7]O. O. Abudayyeh and J. S. Gootenberg, "CRISPR diagnostics," *Science,* vol. 372, no. 6545, pp. 914-915, 2021.

[8]D. S. Chertow, "Next-generation diagnostics with CRISPR," *science,* vol. 360, no. 6387, pp. 381-382, 2018.

[9]M. M. Kaminski, O. O. Abudayyeh, J. S. Gootenberg, F. Zhang, and J. J. Collins, "CRISPR-based diagnostics," *Nature Biomedical Engineering,* vol. 5, no. 7, pp. 643-656, 2021.

[10] H. Yue, M. Huang, T. Tian, E. Xiong, and X. Zhou, "Advances in clustered, regularly interspaced short palindromic repeats (CRISPR)-based diagnostic assays assisted by micro/nanotechnologies," *ACS nano,* vol. 15, no. 5, pp. 7848-7859, 2021.

[11] J. P. Broughton *et al.*, "CRISPR–Cas12-based detection of SARS-CoV-2," *Nature biotechnology,* vol. 38, no. 7, pp. 870-874, 2020.

[12] J. S. Gootenberg *et al.*, "Nucleic acid detection with CRISPR-Cas13a/C2c2," *Science,* vol. 356, no. 6336, pp. 438-442, 2017.

[13] M. J. Kellner, J. G. Koob, J. S. Gootenberg, O. O. Abudayyeh, and F. Zhang, "SHERLOCK: nucleic acid detection with CRISPR nucleases," *Nature protocols,* vol. 14, no. 10, pp. 2986-3012, 2019.

[14] S.-Y. Li *et al.*, "CRISPR-Cas12a-assisted nucleic acid detection," *Cell discovery,* vol. 4, no. 1, pp. 1-4, 2018.

[15] W. E. Huang *et al.*, "RT‐LAMP for rapid diagnosis of coronavirus SARS‐CoV‐2," *Microbial biotechnology,* vol. 13, no. 4, pp. 950-961, 2020.

[16] G. J. Knott and J. A. Doudna, "CRISPR-Cas guides the future of genetic engineering," *Science,* vol. 361, no. 6405, pp. 866-869, 2018.

[17] H. de Puig *et al.*, "Minimally instrumented SHERLOCK (miSHERLOCK) for CRISPR-based point-of-care diagnosis of SARS-CoV-2 and emerging variants," *Science Advances,* vol. 7, no. 32, p. eabh2944, 2021.

[18] X. Xiang, Y. Shang, J. Zhang, Y. Ding, and Q. Wu, "Advances in improvement strategies of digital nucleic acid amplification for pathogen detection," *TrAC Trends in Analytical Chemistry,* p. 116568, 2022.

[19] R. Nouri, M. Dong, A. J. Politza, and W. Guan, "Figure of Merit for CRISPR-Based Nucleic Acid-Sensing Systems: Improvement Strategies and Performance Comparison," *ACS sensors,* vol. 7, no. 3, pp. 900-911, 2022.

[20] R. Yao, D. Liu, X. Jia, Y. Zheng, W. Liu, and Y. Xiao, "CRISPR-Cas9/Cas12a biotechnology and application in bacteria," *Synthetic and Systems Biotechnology,* vol. 3, no. 3, pp. 135-149, 2018.
[21] J. S. Chen *et al.*, "CRISPR-Cas12a target binding unleashes indiscriminate single-stranded DNase activity," *Science,* vol. 360, no. 6387, pp. 436-439, 2018.
[22] J. Dronina, U. Samukaite-Bubniene, and A. Ramanavicius, "Towards application of CRISPR-Cas12a in the design of modern viral DNA detection tools," *Journal of Nanobiotechnology,* vol. 20, no. 1, pp. 1-15, 2022.
[23] O. O. Abudayyeh *et al.*, "RNA targeting with CRISPR–Cas13," *Nature,* vol. 550, no. 7675, pp. 280-284, 2017.
[24] O. O. Abudayyeh *et al.*, "C2c2 is a single-component programmable RNA-guided RNA-targeting CRISPR effector," *Science,* vol. 353, no. 6299, p. aaf5573, 2016.
[25] A. Ramachandran and J. G. Santiago, "CRISPR enzyme kinetics for molecular diagnostics," *Analytical Chemistry,* vol. 93, no. 20, pp. 7456-7464, 2021.
[26] S.-Y. Li, Q.-X. Cheng, J.-K. Liu, X.-Q. Nie, G.-P. Zhao, and J. Wang, "CRISPR-Cas12a has both cis-and trans-cleavage activities on single-stranded DNA," *Cell research,* vol. 28, no. 4, pp. 491-493, 2018.
[27] Y. Li, S. Li, J. Wang, and G. Liu, "CRISPR/Cas systems towards next-generation biosensing," *Trends in biotechnology,* vol. 37, no. 7, pp. 730-743, 2019.
[28] P. G. Maass, A. R. Barutcu, D. M. Shechner, C. L. Weiner, M. Melé, and J. L. Rinn, "Spatiotemporal allele organization by allele-specific CRISPR live-cell imaging (SNP-CLING)," *Nature structural & molecular biology,* vol. 25, no. 2, pp. 176-184, 2018.
[29] R. Barrangou and J. A. Doudna, "Applications of CRISPR technologies in research and beyond," *Nature biotechnology,* vol. 34, no. 9, pp. 933-941, 2016.
[30] J. S. Gootenberg, O. O. Abudayyeh, M. J. Kellner, J. Joung, J. J. Collins, and F. Zhang, "Multiplexed and portable nucleic acid detection platform with Cas13, Cas12a, and Csm6," *Science,* vol. 360, no. 6387, pp. 439-444, 2018.
[31] Z. Ali *et al.*, "iSCAN: An RT-LAMP-coupled CRISPR-Cas12 module for rapid, sensitive detection of SARS-CoV-2," *Virus research,* vol. 288, p. 198129, 2020.
[32] S. Kannan *et al.*, "Compact RNA editors with small Cas13 proteins," *Nature biotechnology,* vol. 40, no. 2, pp. 194-197, 2022.
[33] C. Myhrvold *et al.*, "Field-deployable viral diagnostics using CRISPR-Cas13," *Science,* vol. 360, no. 6387, pp. 444-448, 2018.
[34] L. B. Harrington *et al.*, "Programmed DNA destruction by miniature CRISPR-Cas14 enzymes," *Science,* vol. 362, no. 6416, pp. 839-842, 2018.
[35] H. Noji, Y. Minagawa, and H. Ueno, "Enzyme-based digital bioassay technology–Key strategies and future perspectives," *Lab on a Chip,* 2022.
[36] A. S. Basu, "Digital assays part I: partitioning statistics and digital PCR," *SLAS technology,* vol. 22, no. 4, pp. 369-386, 2017.
[37] P. R. Debski and P. Garstecki, "Designing and interpretation of digital assays: Concentration of target in the sample and in the source of sample," *Biomolecular detection and quantification,* vol. 10, pp. 24-30, 2016.
[38] P. Zhu and L. Wang, "Passive and active droplet generation with microfluidics: a review," *Lab on a Chip,* vol. 17, no. 1, pp. 34-75, 2017.
[39] S. Dube, J. Qin, and R. Ramakrishnan, "Mathematical analysis of copy number variation in a DNA sample using digital PCR on a nanofluidic device," *PloS one,* vol. 3, no. 8, p. e2876,

2008.
[40] L. B. Pinheiro *et al.*, "Evaluation of a droplet digital polymerase chain reaction format for DNA copy number quantification," *Analytical chemistry,* vol. 84, no. 2, pp. 1003-1011, 2012.
[41] G. S. Yen, B. S. Fujimoto, T. Schneider, J. E. Kreutz, and D. T. Chiu, "Statistical analysis of nonuniform volume distributions for droplet-based digital PCR assays," *Journal of the American Chemical Society,* vol. 141, no. 4, pp. 1515-1525, 2019.
[42] A. Bar-Even *et al.*, "The moderately efficient enzyme: evolutionary and physicochemical trends shaping enzyme parameters," *Biochemistry,* vol. 50, no. 21, pp. 4402-4410, 2011.
[43] Z. Hu *et al.*, "A novel method based on a Mask R-CNN model for processing dPCR images," *Analytical Methods,* vol. 11, no. 27, pp. 3410-3418, 2019.
[44] L. Shang, Y. Cheng, and Y. Zhao, "Emerging droplet microfluidics," *Chemical reviews,* vol. 117, no. 12, pp. 7964-8040, 2017.
[45] S.-Y. Teh, R. Lin, L.-H. Hung, and A. P. Lee, "Droplet microfluidics," *Lab on a Chip,* vol. 8, no. 2, pp. 198-220, 2008.
[46] X. Luo *et al.*, "Digital CRISPR/Cas12b-based platform enabled absolute quantification of viral RNA," *Analytica Chimica Acta,* vol. 1192, p. 339336, 2022.
[47] T. Tian *et al.*, "An ultralocalized Cas13a assay enables universal and nucleic acid amplification-free single-molecule RNA diagnostics," *ACS nano,* vol. 15, no. 1, pp. 1167-1178, 2020.
[48] H. Yue *et al.*, "Droplet Cas12a assay enables DNA quantification from unamplified samples at the single-molecule level," *Nano Letters,* vol. 21, no. 11, pp. 4643-4653, 2021.
[49] F. X. Liu *et al.*, "Isothermal Background-Free Nucleic Acid Quantification by a One-Pot Cas13a Assay Using Droplet Microfluidics," *Analytical Chemistry,* vol. 94, no. 15, pp. 5883-5892, 2022.
[50] T. Yu, S. Zhang, R. Matei, W. Marx, C. L. Beisel, and Q. Wei, "Coupling smartphone and CRISPR–Cas12a for digital and multiplexed nucleic acid detection," *AIChE Journal,* vol. 67, no. 12, p. e17365, 2021.
[51] H. Shinoda *et al.*, "Automated amplification-free digital RNA detection platform for rapid and sensitive SARS-CoV-2 diagnosis," *Communications Biology,* vol. 5, no. 1, pp. 1-8, 2022.
[52] H. Shinoda *et al.*, "Amplification-free RNA detection with CRISPR–Cas13," *Communications biology,* vol. 4, no. 1, pp. 1-7, 2021.
[53] S. Son *et al.*, "Sensitive and multiplexed RNA detection with Cas13 droplets and kinetic barcoding," *MedRXiv,* 2021.
[54] X. Wu, C. Chan, S. L. Springs, Y. H. Lee, T. K. Lu, and H. Yu, "A warm-start digital CRISPR/Cas-based method for the quantitative detection of nucleic acids," *Analytica Chimica Acta,* vol. 1196, p. 339494, 2022.
[55] X. Ding, K. Yin, Z. Li, M. M. Sfeir, and C. Liu, "Sensitive quantitative detection of SARS-CoV-2 in clinical samples using digital warm-start CRISPR assay," *Biosensors and Bioelectronics,* vol. 184, p. 113218, 2021.
[56] W. Du, L. Li, K. P. Nichols, and R. F. Ismagilov, "SlipChip," *Lab on a Chip,* vol. 9, no. 16, pp. 2286-2292, 2009.
[57] F. Shen, W. Du, J. E. Kreutz, A. Fok, and R. F. Ismagilov, "Digital PCR on a SlipChip," *Lab on a Chip,* vol. 10, no. 20, pp. 2666-2672, 2010.
[58] Z. Yu *et al.*, "Self-partitioning SlipChip for slip-induced droplet formation and human papillomavirus viral load quantification with digital LAMP," *Biosensors and Bioelectronics,* vol. 155, p. 112107, 2020.

[59] Z. Yu, L. Xu, W. Lyu, and F. Shen, "Parallel Multistep Digital Analysis SlipChip Demonstrated with the Quantification of Nucleic Acid by Digital LAMP-CRISPR," *Lab on a Chip,* 2022.
[60] J. S. Park, K. Hsieh, L. Chen, A. Kaushik, A. Y. Trick, and T. H. Wang, "Digital CRISPR/Cas‐Assisted assay for rapid and sensitive detection of SARS‐CoV‐2," *Advanced Science,* vol. 8, no. 5, p. 2003564, 2021.
[61] H. Wu *et al.*, "DropCRISPR: A LAMP-Cas12a based digital method for ultrasensitive detection of nucleic acid," *Biosensors and Bioelectronics,* p. 114377, 2022.
[62] X. Wu *et al.*, "Digital CRISPR-based method for the rapid detection and absolute quantification of nucleic acids," *Biomaterials,* vol. 274, p. 120876, 2021.
[63] C. M. Ackerman *et al.*, "Massively multiplexed nucleic acid detection with Cas13," *Nature,* vol. 582, no. 7811, pp. 277-282, 2020.
[64] R. Bruch, G. A. Urban, and C. Dincer, "CRISPR/Cas powered multiplexed biosensing," *Trends in biotechnology,* vol. 37, no. 8, pp. 791-792, 2019.
[65] T. Gou *et al.*, "Smartphone-based mobile digital PCR device for DNA quantitative analysis with high accuracy," *Biosensors and Bioelectronics,* vol. 120, pp. 144-152, 2018.
[66] F. Hu *et al.*, "Smartphone-based droplet digital LAMP device with rapid nucleic acid isolation for highly sensitive point-of-care detection," *Analytical chemistry,* vol. 92, no. 2, pp. 2258-2265, 2019.
[67] X. Lin, X. Huang, K. Urmann, X. Xie, and M. R. Hoffmann, "Digital loop-mediated isothermal amplification on a commercial membrane," *ACS sensors,* vol. 4, no. 1, pp. 242-249, 2019.
[68] Y. Shan, X. Zhou, R. Huang, and D. Xing, "High-fidelity and rapid quantification of miRNA combining crRNA programmability and CRISPR/Cas13a trans-cleavage activity," *Analytical chemistry,* vol. 91, no. 8, pp. 5278-5285, 2019.
[69] D. A. Huyke, A. Ramachandran, V. I. Bashkirov, E. K. Kotseroglou, T. Kotseroglou, and J. G. Santiago, "Enzyme Kinetics and Detector Sensitivity Determine Limits of Detection of Amplification-Free CRISPR-Cas12 and CRISPR-Cas13 Diagnostics," *Analytical Chemistry,* vol. 94, no. 27, pp. 9826-9834, 2022.
[70] C. Sun, L. Liu, H. N. Vasudevan, K.-C. Chang, and A. R. Abate, "Accurate Bulk Quantitation of Droplet Digital Polymerase Chain Reaction," *Analytical chemistry,* vol. 93, no. 29, pp. 9974-9979, 2021.